Probing a protein–protein interaction by *in vitro* evolution

George Thom, Alexis C. Cockroft, Andrew G. Buchanan, Cathy Joberty Candotti, E. Suzanne Cohen, David Lowne, Phill Monk, Celia P. Shorrock-Hart, Lutz Jermutus, and Ralph R. Minter*

Cambridge Antibody Technology, Milstein Building, Granta Park, Cambridge CB1 6GH, United Kingdom

Communicated by Aaron Klug, Medical Research Council, Cambridge, United Kingdom, March 24, 2006 (received for review December 2, 2005)

In this study, we used *in vitro* protein evolution with ribosome and phage display to optimize the affinity of a human IL-13-neutralizing antibody, a therapeutic candidate for the treatment of asthma, >150-fold to 81 pM by using affinity-driven stringency selections. Simultaneously, the antibody potency to inhibit IL-13-dependent proliferation in a cell-based functional assay increased 345-fold to an IC_{50} of 229 pM. The panoply of different optimized sequences resulting from complementarity-determining region-targeted mutagenesis and error-prone PCR using ribosome display was contrasted with that of complementarity-determining region-targeted mutagenesis alone using phage display. The data highlight the advantage of the ribosome-display approach in identifying beneficial mutations across the entire sequence space. A comparison of mutation hotspots from *in vitro* protein evolution to knockout mutations from alanine scanning demonstrated that *in vitro* evolution selects the most appropriate positions for improvements in potency without mutating any of the key residues within the functional paratope.

affinity maturation | human antibodies | IL-13 | protein evolution | ribosome display

With the advent of new and robust methods to isolate fully human or humanized monoclonal antibodies against a wide variety of clinically relevant targets there has been a significant rise in the number of therapeutic antibodies in clinical trials (for a review, see ref. 1). Because it is generally possible to isolate antibodies against defined disease targets, the emphasis has shifted toward optimizing the potency and other features of antibodies to improve the pharmacology and therapeutic efficacy. The majority of these antibody engineering projects have concentrated on improving antibody affinity *in vitro* to achieve potency gains *in vivo*, and the increasing number of antibody engineering projects being undertaken is beginning to yield rational explanations for observed potency gains (2, 3).

Many different mutagenesis strategies have been used to improve the potency of candidate therapeutic antibodies. These strategies range from random mutagenesis of the entire Fv sequence to the targeting of mutations to the complementarity-determining region (CDR) loops, where the chance of influencing antibody potency is believed to be higher. Saturation mutagenesis of all CDR loop residues is made impossible by the sheer number of potential combinations of amino acids that must be explored. Despite the production of large (10^9-10^{12}) variant libraries becoming a more accessible procedure, this allows the full exploration of only six or seven residues. As a result, a large number of affinity maturation approaches have just focused on the region with the highest likelihood of yielding favorable affinity gains, V_H CDR3. The desirable approach of performing structure analysis of Fv regions *in silico* and "designing" improved CDR loops is not yet achievable, despite the availability of a relatively large number of high-resolution antibody crystal structures. The main reason for this barrier is the current inability of modeling software to account for loop flexibility and also the kind of changes that occur during the binding event, such as those associated with "induced fit" binding (4, 5). It has been proposed that, during affinity maturation *in vivo*, germ-line antibodies, which are capable of major structural changes upon complex formation and can therefore bind multiple antigens, are "fixed" into a more rigid loop structure with high affinity for a single antigen (6, 7). To date, such conformational changes have been refractory to modeling *in silico* due to the multitude of potential topographies that can be adopted even in a single antibody.

To define the antibody–antigen contact area more precisely and therefore reduce the theoretical diversity of affinity maturation libraries, methods such as alanine scanning and homologue scanning have been used. Empirical determination of the paratope residues by alanine scanning has proven useful in determining which amino acids have an energetically favorable effect on antigen binding (8, 9). During this process, a short list of residues likely to be involved in antigen binding, for example, the CDR loop residues, are mutated to alanine, and the effect resulting from the loss of side-chain moiety is determined. Residues intolerant of alanine replacement are considered to be those that make energetically favorable contacts with antigen and thus define the functional paratope. Incidentally, the energetic paratope identified by such mutagenesis methods does not necessarily coincide with the topological paratope as determined by x-ray crystallography and can identify buried residues that serve to stabilize the antibody conformation rather than the antibody–antigen complex (10). Homologue scanning, an alternative method that involves replacement of wild-type residues with amino acids having similar side-chain chemistries, is thought to further define a subset of paratope residues that are an absolute requirement for antigen binding (9). In the majority of cases, it has been concluded that residues within the functional paratope should not be randomized for improved potency, because they are likely to be intolerant of any amino acid substitutions (11, 12). Alanine and homologue scanning are therefore reliable methods to determine which residues to avoid mutating during the process of antibody optimization.

However, a more useful method to inform and direct antibody affinity maturation would be one that rapidly identified positions where change is tolerated and usually associated with affinity gains. One technique that has the potential to yield this type of information is random mutagenesis coupled with Fv display technologies (13, 14). In this strategy, the whole Fv sequence is mutagenized by either error-prone PCR or mutagenic *Escherichia coli* strains, and then the library of variants is selected or screened for improved affinity. Additional cycles of mutagenesis and selection can be applied to favor the accumulation of beneficial mutations in the pool of selected variants, and, by

Conflict of interest statement: G.T., A.C.C., A.G.B., C.J.C., E.S.C., D.L., P.M., C.P.S.-H., L.J., and R.R.M. are employees of Cambridge Antibody Technology Ltd.

Freely available online through the PNAS open access option.

Abbreviations: CDR, complementarity-determining region; scFv, single-chain Fv.

*To whom correspondence should be addressed. E-mail: ralph.minter@cambridgeantibody.com.

BIOCHEMISTRY

analyzing the sequences of clones with improved potency, a map of hotspots can be derived that is effectively a functional scan of the Fv sequence. *In vitro* display technologies, such as ribosome display, offer two important advantages. First, large libraries can be made rapidly, because there is no need to transform large numbers of mutant plasmids into a host; and second, additional mutations can be introduced at every round, because a PCR step is included in each selection cycle rather than an *in vivo* amplification step.

In this study, H-chain CDR3-targeted mutagenesis and phage display were used to engineer a 200-fold potency gain in a neutralizing human antibody against IL-13, allowing this antibody to progress as a clinical candidate for the treatment of asthma. In a parallel approach using ribosome display, iterative cycles of random mutagenesis were used not only to isolate the same high-affinity antibody as in the first approach but also to map out areas of the antibody surface that were tolerant of amino acid replacement. Interestingly, the clusters of mutations highlighted by *in vitro* evolution did not show any significant overlap with amino acid residues shown by alanine scanning to contribute significantly to binding energy. Scanning of protein sequence space by using iterative cycles of random mutagenesis and *in vitro* selection is therefore a rapid way to gain knowledge about the protein interaction surface, which can be used to inform a targeted mutagenesis strategy, hence, enabling a semi-rational approach to antibody affinity optimization.

Results

V_H CDR3 Affinity Maturation. The affinity maturation of the IL-13-neutralizing antibody BAK1 was performed by *in vitro* evolution by using both phage and ribosome display. The phage display strategy was to perform saturation mutagenesis of the V_H CDR3 region by creating three libraries, each randomizing a different, continuous block of six amino acids. The resulting library sizes were all $>1 \times 10^9$, indicating that all combinations of amino acids were theoretically represented within each block of six amino acids. The mutant libraries were expressed as single-chain Fv (scFv) on the surface of phage and selected for improved affinity on decreasing concentrations of biotinylated IL-13, reducing 10-fold at each round, from 10 nM at round 1 to 100 pM at round 3. For an initial ranking, variants from these selection outputs were prepared as scFv and assayed for potency improvements over BAK1 in an IL-13-dependent TF-1 cell proliferation assay. Four variants with improved potency over BAK1 were identified in this initial screen, and a single variant, BAK1.1, showed a 5-fold improvement in IC_{50} value as scFv, from 44 nM to 8 nM (Table 1). It was of interest to note that, despite the large number of variants created by V_H CDR3 randomization, the sequence of BAK1.1 contained only two amino acid mutations from BAK1. A single amino acid substitution (V_H N99S) was seen in V_H CDR3, and a point mutation, presumably resulting from a polymerase error during library construction, was found in V_L CDR1 (V_L N27I). The V_L CDR1 change at L27 inserts an amino acid, isoleucine, which is not observed in any of the germ-line λ or κ sequences at that position.

Ribosome Display Affinity Maturation. Library design for ribosome display was identical to that used for phage display in that three regions of six amino acids within V_H CDR3 were fully randomized. More mutations were introduced by incorporating error-prone PCR amplification of the scFv sequences before rounds 1 and 3 of selection. Ribosome display was performed by using decreasing concentrations of IL-13, reducing 10-fold at each round, from 10 nM at round 1 down to 100 pM at round 3. Unique variant scFvs were tested for improved potency over BAK1 scFv in the TF-1 proliferation assay. Surprisingly, the variant BAK1.1, with the V_H N99S and V_L N27I mutations, was also isolated by using ribosome display. The ribosome display approach yielded 24 additional variants (BAK1.5 to BAK1.28) with IC_{50} values of between 4.3 and 23 nM in the TF-1 proliferation assay (Table 1), which were therefore between 2- and 10-fold improved over BAK1. The V_H N99S mutation was strongly selected, as judged by its appearance in 10 of the 25 mutants shown. As with phage display selections, very few beneficial changes were observed in V_H CDR3, with only one other position (V_H S97N) mutated from wild type in the improved mutant population. Error-prone PCR added an average of three mutations per improved variant after selection and screening. V_L CDR1, in particular, accumulated a disproportionately large number of changes (25 of 75 error-prone mutations were found in V_L CDR1). The distribution of mutations shows a very strong preference for CDR mutations over framework changes, with 63 of 75 (84%) error-prone PCR mutations occurring in CDRs. This finding is illustrated in Fig. 1, which plots the mutation rate observed in the ribosome display-selected variants against data recorded for mutations resulting from somatic hypermutation *in vivo* (15, 16).

CDR Walking Mutagenesis in V_H CDR1 and V_H CDR2. To further optimize the potency of the BAK1.1 scFv, a CDR walking approach was evaluated. The BAK1.1 sequence, with mutations already accumulated in V_H CDR3 and V_L CDR1, was subjected to saturation mutagenesis at selected residues in V_H CDR1 and V_H CDR2. The choice of residues was based on the mutational hotspots identified by the previous *in vitro* evolution together with a study of antibody–antigen crystal structures detailing the frequency at which given amino acid side chains in the antibody-combining site are in close proximity to antigen (17). After selection by phage display and screening, 8 variants with picomolar IC_{50} values as scFv in the TF-1 assay were isolated from the V_H CDR1 library, and 18 variants, also with picomolar IC_{50} values, were isolated from the V_H CDR2 library, 2 of which contained spontaneous mutations in V_H CDR1 (Table 1). Most of these optimized variants appear to have derived a further gain in potency by combining novel V_H CDR1 or V_H CDR2 mutations with the existing mutations in V_H CDR3 and V_L CDR1.

Potency and Affinity Determinations. Variant BAK1.1, isolated in both the phage and ribosome display affinity maturation approaches, was converted to an IgG4 molecule along with the BAK1.29 and BAK1.45 variants from the V_H CDR1 and V_H CDR2 CDR walking strategies, respectively. All variant IgG4 antibodies were tested for potency against the BAK1 IgG4 antibody in the TF-1 proliferation assay, and the affinities were determined by kinetic analysis using surface plasmon resonance (Fig. 2 and Table 2). The largest gain in potency and affinity was demonstrated by the BAK1.45 variant, which had an IC_{50} value of 229 pM in the TF-1 assay and a K_d of 81 pM. This result corresponded to an overall improvement of 345-fold in potency and 167-fold in affinity relative to the parental BAK1 antibody. The BAK1.1 variant, derived by both phage display and ribosome display, was itself significantly improved relative to the BAK1 parent antibody, with an increase of 203-fold in potency and 82-fold in affinity. The potency gain upon conversion from scFv to IgG for BAK1.1 was 21-fold, whereas for BAK1.29 and BAK1.45 there was no potency gain upon conversion. This finding probably reflects an increase in stability for BAK1.29 and BAK1.45 in scFv format compared with BAK1.1, because the conditions of the TF-1 proliferation assay (37°C for 72 h) would be expected to expose any differences in scFv stability without affecting the activity of molecules in the more stable IgG format.

Visualization of Key Mutations in a Structural Model of BAK1.1 Fv. A model of the BAK1.1 V region structure was used to visualize the topographical location of the residues mutated during the af-

Table 1. Alignment of CDR sequences of BAK1 variants with improved potency derived by *in vitro* evolution

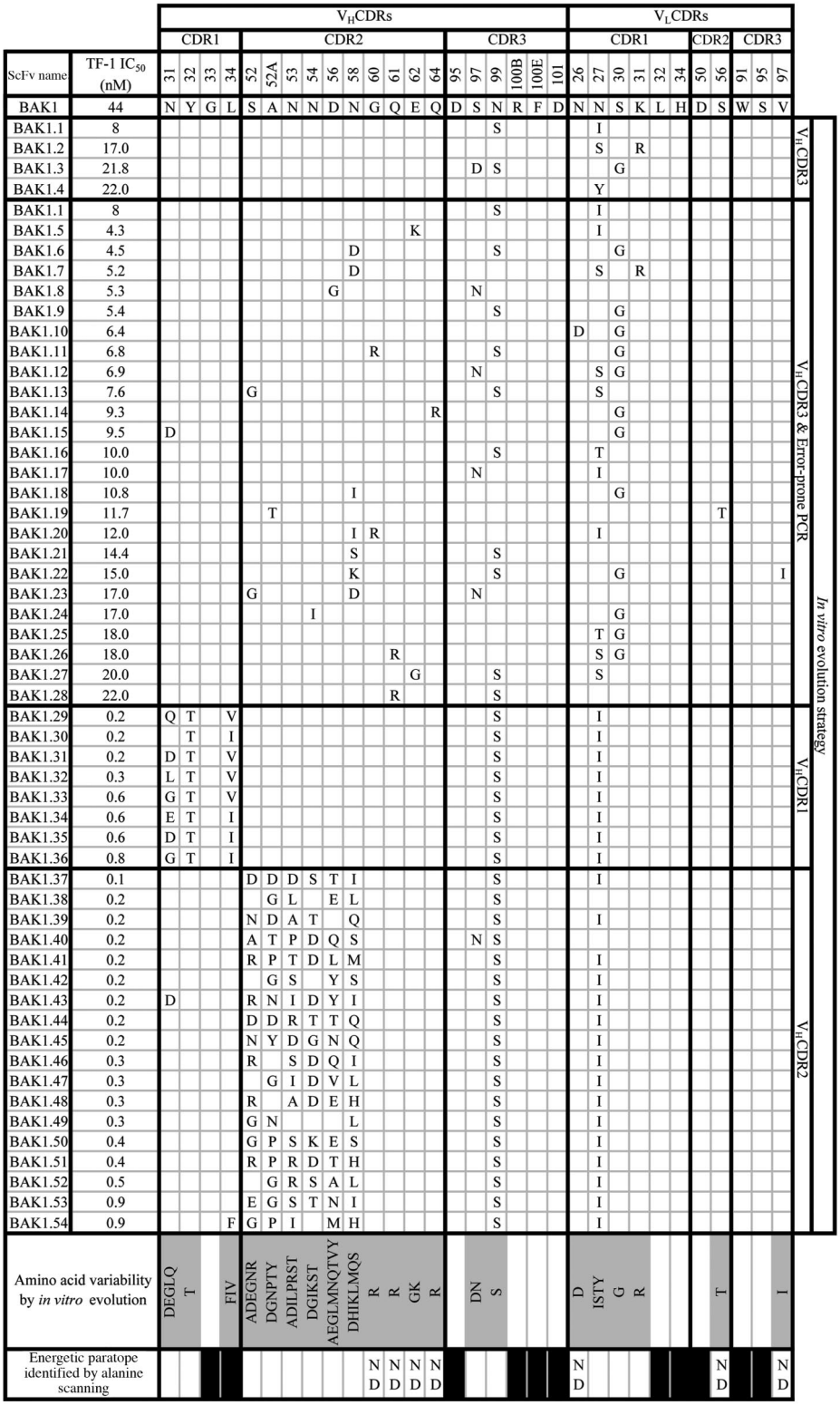

		V_HCDRs																				V_LCDRs												
		CDR1				CDR2									CDR3							CDR1						CDR2		CDR3				
ScFv name	TF-1 IC_{50} (nM)	31	32	33	34	52	52A	53	54	56	58	60	61	62	64	95	97	99	100B	100E	101	26	27	30	31	32	34	50	56	91	95	97		
BAK1	44	N	Y	G	L	S	A	N	N	D	N	G	Q	E	Q	D	S	N	R	F	D	N	N	S	K	L	H	D	S	W	S	V		
BAK1.1	8																	S					I										V_HCDR3	*In vitro* evolution strategy
BAK1.2	17.0																						S		R									
BAK1.3	21.8																D	S						G									
BAK1.4	22.0																						Y											
BAK1.1	8																	S					I										V_HCDR3 & Error-prone PCR	
BAK1.5	4.3													K									I											
BAK1.6	4.5										D							S						G									
BAK1.7	5.2										D												S		R									
BAK1.8	5.3									G							N																	
BAK1.9	5.4																	S						G										
BAK1.10	6.4																					D		G										
BAK1.11	6.8											R						S						G										
BAK1.12	6.9																N						S	G										
BAK1.13	7.6					G												S					S											
BAK1.14	9.3														R									G										
BAK1.15	9.5	D																						G										
BAK1.16	10.0																	S					T											
BAK1.17	10.0																N						I											
BAK1.18	10.8										I													G										
BAK1.19	11.7						T																						T					
BAK1.20	12.0										I	R											I											
BAK1.21	14.4										S							S																
BAK1.22	15.0										K							S						G									I	
BAK1.23	17.0					G					D						N																	
BAK1.24	17.0								I															G										
BAK1.25	18.0																						T	G										
BAK1.26	18.0												R										S	G										
BAK1.27	20.0													G				S					S											
BAK1.28	22.0												R					S																
BAK1.29	0.2	Q	T		V													S					I										V_HCDR1	
BAK1.30	0.2		T		I													S					I											
BAK1.31	0.2	D	T		V													S					I											
BAK1.32	0.3	L	T		V													S					I											
BAK1.33	0.6	G	T		V													S					I											
BAK1.34	0.6	E	T		I													S					I											
BAK1.35	0.6	D	T		I													S					I											
BAK1.36	0.8	G	T		I													S					I											
BAK1.37	0.1					D	D	D	S	T	I							S					I										V_HCDR2	
BAK1.38	0.2						G	L		E	L							S																
BAK1.39	0.2					N	D	A	T		Q							S					I											
BAK1.40	0.2					A	T	P	D	Q	S						N	S																
BAK1.41	0.2					R	P	T	D	L	M							S					I											
BAK1.42	0.2						G	S		Y	S							S					I											
BAK1.43	0.2	D				R	N	I	D	Y	I							S					I											
BAK1.44	0.2					D	D	R	T	T	Q							S					I											
BAK1.45	0.2					N	Y	D	G	N	Q							S					I											
BAK1.46	0.3					R		S	D	Q	I							S					I											
BAK1.47	0.3						G	I	D	V	L							S					I											
BAK1.48	0.3					R		A	D	E	H							S					I											
BAK1.49	0.3					G	N				L							S					I											
BAK1.50	0.4					G	P	S	K	E	S							S					I											
BAK1.51	0.4					R	P	R	D	T	H							S					I											
BAK1.52	0.5						G	R	S	A	L							S					I											
BAK1.53	0.9					E	G	S	T	N	I							S					I											
BAK1.54	0.9				F	G	P	I		M	H							S					I											
Amino acid variability by *in vitro* evolution		DEGLQ T			FIV	ADEGNR	DGNPTY	ADILPRST	DGIKST	AEGLMNQTVY	DHIKLMQS	R	R	GK	R		DN	S				D	ISTY	G	R			T		I				
Energetic paratope identified by alanine scanning												N D	N D	N D	N D							N D						N D			N D			

CDR differences from the parental BAK1 sequence that resulted in improved potency are shown. Shown on the right is the *in vitro* evolution strategy by which the variants were derived. The neutralizing potency, as measured by the IC_{50} (nanomolar concentration) as scFv in the IL-13-dependent TF-1 cell proliferation assay, is shown for BAK1 and all variants. All TF-1 IC_{50} figures were calculated from samples analyzed in triplicate, and all values had standard deviations of $<10\%$. Note that variant BAK1.1 was derived independently both by phage and by ribosome display technology. In addition, the table summarizes amino acid variability for each CDR position after *in vitro* evolution and the residues found to constitute the energetic paratope as determined by alanine scanning. Amino acid numbering and CDRs are assigned according to Kabat *et al.* (20). ND, not determined.

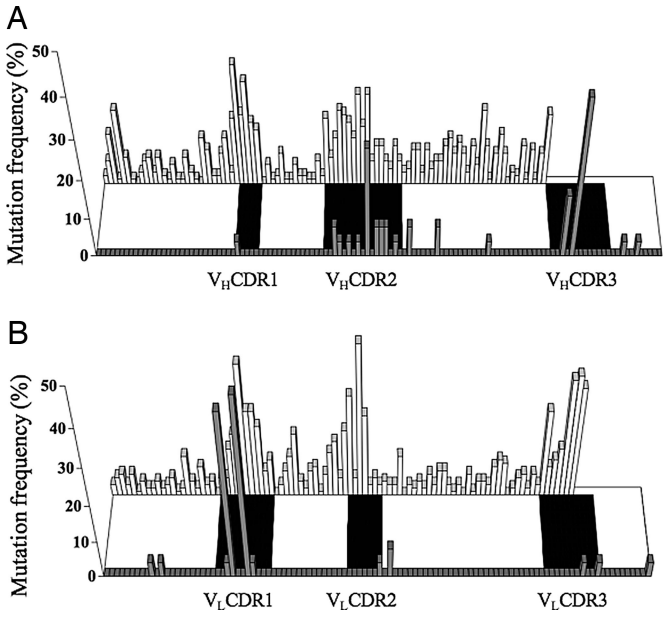

Fig. 1. Comparison of the amino acid substitution frequency after affinity maturation of BAK1 by using ribosome display and the frequency observed after somatic hypermutation of human antibody sequences *in vivo*. Mutation frequencies for ribosome display (gray bars) and *in vivo* hypermutation (white bars) are shown for the V_H region (*A*) and the V_L region (*B*), with CDRs marked. Somatic hypermutation data are unavailable for CDR3 and framework 4 of both the V_H and V_L regions, and these sections are excluded from analysis. *In vivo* somatic hypermutation frequencies are reproduced from refs. 15 and 16.

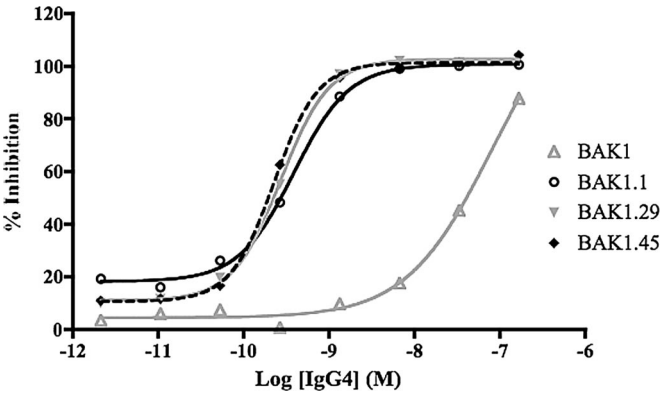

Fig. 2. Inhibition of IL-13-induced proliferation in TF-1 cells by the anti-IL-13 parent IgG4 BAK1 (IC_{50} of 78.9 nM) and the optimized IgG4 variants BAK1.1 (IC_{50} of 388 pM), BAK1.29 (IC_{50} of 274 pM), and BAK1.45 (IC_{50} of 229 pM). To obtain an IC_{50}, triplicate titrations of IgG4 were preincubated with recombinant human IL-13 before both were added to TF-1 cells, and levels of cell proliferation were measured by uptake of tritiated thymidine.

finity maturation process. For the purposes of this visual analysis, residues were termed mutational hotspots if they were found independently in two variants with improved potency, which corresponds to a mutation frequency of ≥3.5% in the population of improved variants. Seventeen CDR positions were identified as mutational hotspots by *in vitro* evolution, primarily by using ribosome display, and show a wide distribution over the variable region surface, encompassing changes in four CDRs. In contrast, the 11 residues that are thought to make up the functional paratope, as deduced from the alanine-scanning study, show no overlap with the ribosome display hotspot positions, with the exception of residue 34 in V_H CDR1. This position, which is a leucine in the original BAK1 antibody, appears almost totally buried in the structural model and was found to tolerate replacement only with other hydrophobic residues during *in vitro* evolution. This finding suggests that V_H residue 34 plays a role in driving the folding of the scFv molecule, rather than being a true functional paratope residue, and as such is an example of a "false positive" identified through alanine scanning as reported in ref. 10. The remaining 10 residues that make up the paratope are within 4 Å of their nearest neighbor, which results in the paratope forming a densely packed region located in the center of the combining site. Conversely, the hotspot mutations are distributed more widely around the periphery of the combining site, with an average distance of 9 Å between neighboring hotspots (Fig. 3).

Discussion

In vitro evolution by phage display and ribosome display independently isolated an antibody, BAK1.1, of high affinity (a K_d of 164 pM) and high potency (an IC_{50} value of 388 pM in the IL-13-dependent TF-1 cell proliferation assay). The improvement in potency has enabled this antibody to exert an IL-13-neutralizing effect in an allergen-challenge model *in vivo* (P.M., unpublished data) and consequently enabled it to advance into clinical studies for the treatment of asthma. In comparing the two display technologies, it was shown that both are capable of isolating low-frequency but high-affinity variants from large libraries of randomized variants after just three rounds of enrichment. The major advantage of ribosome display is that, because all steps are carried out *in vitro*, there is no need for the laborious step of transformation of the initial library into bacterial cells before selection begins.

Both approaches used randomization of residues in V_H CDR3, and, yet, both highlighted the crucial role of mutations in V_L CDR1 to improve the potency of the IL-13-neutralizing antibody BAK1. This finding highlights a shortcoming in the use of directed mutagenesis alone to improve protein attributes and shows that it would be more helpful to employ a method that can easily and rapidly identify mutational hotspots across the entire sequence space. As a solution to this problem, iterative cycles of ribosome display and random mutagenesis were used to probe

Table 2. Summary of data

scFv	TF-1 IC_{50}, pM	TF-1 IC_{50} BAK1/ TF-1 IC_{50} mutant	k_{on}, $M^{-1}\cdot s^{-1}$	k_{off}, s^{-1}	K_d, pM	K_d BAK1/ K_d mutant
BAK1	78,900	—	5.49×10^5	7.41×10^{-3}	13,500	—
BAK1.1	388	203	2.49×10^6	4.09×10^{-4}	164	82
BAK1.29	274	288	2.99×10^6	4.05×10^{-4}	135	100
BAK1.45	229	345	3.70×10^6	3.00×10^{-4}	81	167

TF-1 IC_{50} data are summarized, along with the binding kinetics of each IgG for IL-13, as measured by surface plasmon resonance. Potency and affinity improvements over BAK1 are also summarized. All TF-1 IC_{50} figures were calculated from samples analyzed in triplicate, and all values, including the kinetic values from surface plasmon resonance, had standard deviations of <10%.

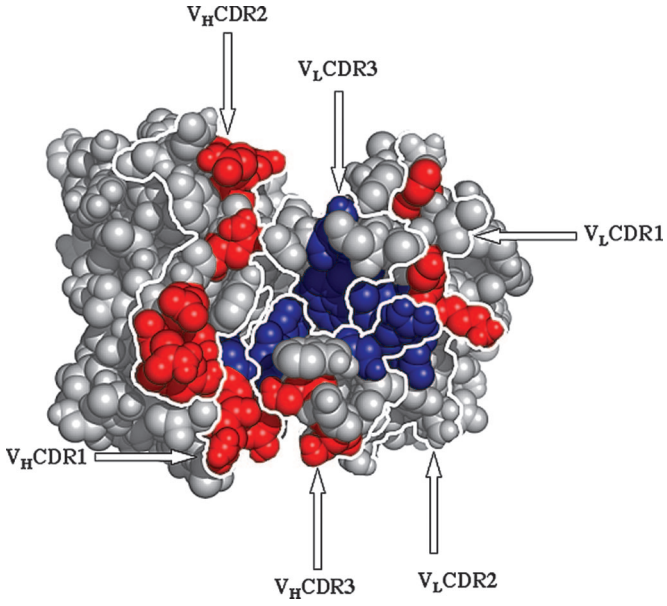

Fig. 3. Mapping of key residues affecting IL-13 binding onto a space-filling structural model of the BAK1.1 Fv from the viewpoint of the antigen. The model shows the V_H chain on the left and the V_L chain on the right, and the six CDRs composing the antigen-combining site are labeled. Hotspot positions (in which residues were found to be mutated independently in two or more variants of improved potency) derived from *in vitro* evolution are shown in red. CDR residues that, upon mutation to alanine, were shown to reduce their maximal binding (R_{max}) to an IL-13-coated Biacore surface by >70%, are shown in dark blue. The two populations show distinct distributions over the antibody V-region surface.

the whole antibody interaction surface for areas tolerant of mutation and where mutation is likely to increase affinity. Because each selection cycle is performed *in vitro*, it can easily be combined with cycles of mutagenesis in an iterative manner to evolve protein characteristics. This scanning approach identified 17 CDR positions in BAK1 that were tolerant of amino acid replacement and associated with improvements in antibody potency. Surprisingly, the frequency of mutations in CDR positions was 84%, with a distribution reminiscent of human antibodies that have undergone somatic hypermutation *in vivo* (Fig. 1). The preference for CDR mutations is strong evidence that the majority of replacements were incorporated because of a beneficial effect on antigen binding, as intended through the use of affinity selections, rather than an effect on protein folding or any other characteristic. The CDR preference is particularly favorable when developing antibodies as therapeutic candidates, because it is desirable for the framework regions to align exactly to the respective human germ-line sequence to reduce the potential for immunogenicity in patients. We observed the CDR preference of mutations resulting from *in vitro* evolution on all five additional antibody optimizations after this study. Although the CDRs constituted only 25% of the total sequence space in the scFvs studied, three of four beneficial mutations (74.5% average) from *in vitro* evolution were in CDR positions (data not shown).

Although the scanning approach is comparable to somatic hypermutation, the advantage of the *in vitro* approach is that, once mutational hotspots have been identified, those key positions can be revisited to introduce the full diversity of amino acid replacements. Both somatic hypermutation and error-prone PCR are limited by the fact that multiple (two to three) base substitutions within a codon are extremely rare. This rarity leads to an inherent bias toward conservative substitutions, and there is some evidence to suggest that nonconservative substitutions can be of significant benefit in the process of protein evolution (18). Furthermore, the pool of hotspots identified in the initial scan is expected to span several noncontinuous regions of sequence space, which could then be randomized in a single library to take advantage of combinatorial effects on potency, where two or more mutations combine synergistically. The *in vitro* nature of ribosome display allows both the initial scan and the follow-up mutagenesis to be carried out rapidly, and, furthermore, the large library sizes available to ribosome display would enable as many as seven hotspots to be investigated in one library.

The combined *in vitro* evolution experiments carried out by using scanning and CDR mutagenesis allowed a large number of mutational hotspots to be identified. At these positions, mutations were frequently associated with improvements in antibody potency. A key question to answer was whether these mutational hotspots coincided with the energetic paratope. By performing an alanine scan of CDR residues, a tight cluster of amino acids in the center of the antigen-binding site was identified as the energetic paratope. Significantly, the *in vitro* evolution experiments identify those residues not in the paratope but in a different population. These tolerated and beneficial mutations were distributed around the periphery of the antigen-combining site, suggesting that their benefit derives not from altering existing side-chain contacts with antigen but by a more subtle approach. This approach could involve several mechanisms, such as altering loop conformation to improve the fit to antigen, the removal of energetically unfavorable side chains in the interface, or an increase in overall charge complementarity with residues in the epitope. The central location of contact residues and the peripheral distribution of maturation hotspots is also in strong agreement with the structural effects seen after the natural affinity maturation process of somatic hypermutation (15, 19). Whatever the exact mechanism for the benefit incurred by the ribosome display-selected mutations may be, the end result was a rapid and informative probing of the antibody surface to identify positions, spanning both CDR and framework regions, where mutations were tolerated and beneficial.

In conclusion, the approach of scanning a protein interaction surface for mutational hotspots is a rapid method to effectively exploit large regions of protein sequence space to identify positions amenable to optimization. The use of ribosome display enables these steps to be performed in a cyclical manner without the need for transformation into bacterial or yeast cells. Furthermore, the approach is broadly applicable and is expected to be especially useful in studying protein–protein interactions and their interfaces.

Materials and Methods

Targeted and Random Antibody Libraries. Three V_H CDR3 libraries, comprising, respectively, randomization of residues 94–99, 98–100C, and 100B–102 (numbered according to Kabat *et al.*, ref. 20), were prepared by oligonucleotide-directed mutagenesis, as described in ref. 21. The V_H CDR1 library, comprising randomization of residues 30–35, and the V_H CDR2 library, comprising randomization of residues 50, 52, 52A, 53, 54, 56, and 58, were also constructed by using oligonucleotide-directed mutagenesis. In between rounds of ribosome display, error-prone PCR was performed on the scFv sequences by using the Diversify mutagenesis kit (Clontech). PCR was performed in the presence of 640 μM $MnSO_4$ and 200 μM dGTP to introduce an average of 8.1 mutations per kilobase of DNA.

Selections. scFv display on phage was achieved by using the phagemid vector pCantab6 (22), and ribosome display of scFv variants was essentially as described in ref. 23. Phage and ribosome display selections for improved affinity were performed in principle according to the published method (24).

Recombinant human IL-13 (PeproTech, Rocky Hill, NJ) was biotinylated by using the reagent biotin disulfide *N*-hydroxysuccinimide ester according to the supplier's recommendations (Pierce) and used in soluble phage and ribosome display selections. To select for higher-affinity scFvs, the concentration of IL-13 was kept below the parent K_d and reduced over three rounds of selection, from 10 nM to 100 pM. The three libraries covering different regions of V_H CDR3 were selected separately at round 1 and then pooled for additional rounds of selection.

Expression of scFv and IgG4 Molecules. Mutant scFv plasmids were cultured in *E. coli*, expression was induced by isopropyl β-D-thiogalactoside, and scFv proteins were isolated from the periplasm by capture of the C-terminal His-tag on Ni^{2+}-nitrilotriacetic acid chromatography, as detailed in ref. 25. Protein concentrations were determined by bicinchoninic acid assay (Sigma). For IgG4 expression, the V_H and V_L chains of selected scFvs were cloned into human IgG4 expression vectors, as described in ref. 26, except that an *oriP* fragment was included in the vectors to facilitate use with human embryonic kidney Epstein–Barr virus-encoded nuclear antigen-293 (HEK EBNA-293) cells and to allow episomal replication. Cotransfection of the H-chain vector pEU8.1(+) and λ L chain vector pEU4.1(−) into HEK EBNA-293 allowed whole IgG4 to be expressed and purified by protein A affinity chromatography (General Electric). Protein concentrations were determined by bicinchoninic acid assay.

IL-13-Dependent TF-1 Cell Proliferation Assay. TF-1 cells (R & D Systems) were maintained in RPMI medium 1640 with GlutaMAX I (Invitrogen) containing 10% fetal bovine serum (JRH Biosciences, Lenexa, KS) and 1% sodium pyruvate (Sigma). Test solutions of scFv or IgG4 were added to human IL-13 (PeproTech) and incubated for 30 min at room temperature before adding to TF-1 cells and incubating at 37°C for 72 h. Ten microliters of tritiated thymidine (50 mCi/ml; 1 Ci = 37 GBq) (NEN) was then added, and the cells were returned to the incubator for another 4 h. Cells were harvested on glass fiber filter plates (PerkinElmer), and thymidine incorporation was determined by using a Packard TopCount microplate liquid scintillation counter. Data were analyzed by using PRISM software (GraphPad, San Diego).

Affinity Determination of IgG4 Antibodies by Biacore Analysis. The affinities of IgG4 antibodies for human IL-13 were determined by surface plasmon resonance measurements by using a Biacore 2000 biosensor, as described in ref. 27. Antibodies were coupled to CM5 sensor chips by using an amine coupling kit (Biacore) at a surface density of ≈500 resonance units, and a serial dilution of IL-13 (PeproTech) from 50 to 0.78 nM in Hepes-buffered saline was passed over the sensor chip surface. The resulting sensorgrams were evaluated by using BIAEVALUATION 3.1 software (Biacore) to provide kinetic data.

Alanine-Scanning Mutagenesis. The alanine scan was performed by changing 41 individual CDR residues in the primary sequence of germ-lined BAK1.1 to alanine by site-directed mutagenesis (the selected V_H residues were 30–35, 50, 52, 52A, 53–58, 95–99, 100A–100C, 100E, and 101–102; and the V_L residues were 27, 29, 30–32, 34, 50, 52–53, and 91–96; numbered according to Kabat *et al.*, ref. 20). These positions were chosen because of a high probability of proximity to antigen, as determined by the study of antibody–antigen crystal structures (17). The maximal binding (R_{max}) of mutant scFv proteins was measured by surface plasmon resonance on a Biacore 2000 Biosensor by using human IL-13 (PeproTech) coupled at high density (500 resonance units) to a CM5 sensor chip. Data were fitted to a 1:1 dissociation model by using the BIAEVALUTION software.

Modeling of Fv Structures. The modeling of the BAK1.1 Fv structure from the primary amino acid sequence was performed by using the web antibody modeling (WAM) algorithm (28). Briefly, the algorithm performed homology modeling by aligning to sequences of antibody V-region x-ray crystal structures stored in the Brookhaven Protein Data Bank to model the V_H and V_L frameworks. CDR loops were then modeled by taking into account the rules for canonical loop structures (28). Visualization of the Fv model was performed by using PYMOL (29).

We thank Jon Large for his help preparing the figures and the DNA Chemistry and High-Throughput Protein Expression teams for their contributions to this work.

1. Brekke, O. H. & Sandlie, I. (2003) *Nat. Rev. Drug Discov.* **2,** 52–62.
2. Yang, P. L. & Schultz, P. G. (1999) *J. Mol. Biol.* **294,** 1191–1201.
3. Gerstner, R. B., Carter, P. & Lowman, H. B. (2002) *J. Mol. Biol.* **321,** 851–862.
4. Carlson, H. A. (2002) *Curr. Opin. Chem. Biol.* **6,** 447–452.
5. Braden, B. C., Fields, B. A., Ysern, X., Goldbaum, F. A., Dall'Acqua, W., Schwarz, F. P., Poljak, R. J. & Mariuzza, R. A. (1996) *J. Mol. Biol.* **257,** 889–894.
6. Yin, J., Mundorff, E. C., Yang, P. L., Wendt, K. U., Hanway, D., Stevens, R. C. & Schultz, P. G. (2001) *Biochemistry* **40,** 10764–10773.
7. Yin, J., Beuscher, A. E., Andryski, S. E., Stevens, R. C. & Schultz, P. G. (2003) *J. Mol. Biol.* **330,** 651–656.
8. Kelley, R. F. & O'Connell, M. P. (1993) *Biochemistry* **32,** 6828–6835.
9. Vajdos, F. F., Adams, C. W., Breece, T. N., Presta, L. G., de Vos, A. M. & Sidhu, S. S. (2002) *J. Mol. Biol.* **320,** 415–428.
10. Greenspan, N. S. & Cooper, L. J. (1995) *Immunol. Today* **16,** 226–230.
11. Lang, S., Xu, J., Stuart, F., Thomas, R. M., Vrijbloed, J. W. & Robinson, J. A. (2000) *Biochemistry* **39,** 15674–15685.
12. Parhami-Seren, B., Viswanathan, M., Strong, R. K. & Margolies, M. N. (2001) *J. Immunol.* **167,** 5129–5135.
13. Boder, E. T., Midelfort, K. S. & Wittrup, K. D. (2000) *Proc. Natl. Acad. Sci. USA* **97,** 10701–10705.
14. Jermutus, L., Honegger, A., Schwesinger, F., Hanes, J. & Plückthun, A. (2001) *Proc. Natl. Acad. Sci. USA* **98,** 75–80.
15. Tomlinson, I. M., Walter, G., Jones, P. T., Dear, P. H., Sonnhammer, E. L. & Winter, G. (1996) *J. Mol. Biol.* **256,** 813–817.
16. Ignatovich, O., Tomlinson, I. M., Jones, P. T. & Winter, G. (1997) *J. Mol. Biol.* **268,** 69–77.
17. MacCallum, R. M., Martin, A. C. & Thornton, J. M. (1996) *J. Mol. Biol.* **262,** 732–745.
18. Miyazaki, K. & Arnold, F. H. (1999) *J. Mol. Evol.* **49,** 716–720.
19. Ramirez-Benitez, M. C. & Almagro, J. C. (2001) *Proteins* **45,** 199–206.
20. Kabat, E. A., Wu, T. T., Perry, H. M., Gottesmann, K. S. & Foeller, C. (1991) *Sequences of Proteins of Immunological Interest* (Natl. Inst. Health, Bethesda), 5th Ed.
21. Baker, K. P., Edwards, B. M., Main, S. H., Choi, G. H., Wager, R. E., Halpern, W. G., Lappin, P. B., Riccobene, T., Abramian, D., Sekut, L., *et al.* (2003) *Arthritis Rheum.* **48,** 3253–3265.
22. McCafferty, J., Fitzgerald, K. J., Earnshaw, J., Chiswell, D. J., Link, J., Smith, R. & Kenten, J. (1994) *Appl. Biochem. Biotechnol.* **47,** 157–171.
23. Hanes, J., Jermutus, L. & Plückthun, A. (2000) *Methods Enzymol.* **328,** 404–430.
24. Hawkins, R. E., Russell, S. J. & Winter, G. (1992) *J. Mol. Biol.* **226,** 889–896.
25. Vaughan, T. J., Williams, A. J., Pritchard, K., Osbourn, J. K., Pope, A. R., Earnshaw, J. C., McCafferty, J., Hodits, R. A., Wilton, J. & Johnson, K. S. (1996) *Nat. Biotechnol.* **14,** 309–314.
26. Persic, L., Roberts, A., Wilton, J., Cattaneo, A., Bradbury, A. & Hoogenboom, H. R. (1997) *Gene* **187,** 9–18.
27. Karlsson, R., Michaelsson, A. & Mattsson, L. (1991) *J. Immunol. Methods* **145,** 229–240.
28. Whitelegg, N. R. & Rees, A. R. (2000) *Protein Eng.* **13,** 819–824.
29. DeLano, W. L. (2002) MACPYMOL (DeLano Scientific, San Carlos, CA), Version 0.98.